Mechanical Properties of Constitutive Parameters in Steel-Concrete Interface

Yong-Hak Lee[1], Young Tae Joo[2], Yeong-Seong Park[3]*, Dong-Ho Ha[4], and Tae-Hyung Lee[5]

Abstract

Mechanical properties of steel-concrete interface are evaluated on the basis of three existing experimental evidences. The properties include bond strength, unbounded and bonded friction angles, residual level of friction angle, mode I fracture energy, mode II bonded fracture energy and unbonded slip-friction energy under different level of normal stress, and shape parameters defining geometrical shape of failure envelope. For this purpose, a typical type of constitutive model of describing steel-concrete interface behavior is presented based on a hyperbolic three-parameter Mohr-Coulom failure criterion. The constitutive model depicts the strong dependency of interface behavior on bonding condition of interface, bonded or unbounded. Mechanical roles of interface parameters are discussed based on the presented interface model. Values of the interface parameters are determined through interpretation of existing experimental results, geometry of failure envelope and sensitivity analyses. These values are applied to push-out tests of concrete-infilled rectangular steel columns with three different cases of interface lengths. Failure process of concrete-infilled rectangular steel column is discussed through comparison of experimental measurements with numerical results.

Keywords: steel-concrete interface, slip and debonding, Mohr-Coulomb failure criterion, fracture energy, elasto-plasticity,

1. Introduction

Numerical prediction of interface behavior using nonlinear finite element framework requires a constitutive model to describe the progressive failure localized into interface region. Numerous research works have been made to model the localized failure process on steel-concrete interface in the lumped manner (Katona (1983), Plesha (1987), Stankowski et al.

[1] Professor, Department of Civil Engineering, Konkuk University, Seoul, Korea
[2] Senior Engineer, MidasIT Co., Seongnam, Korea
[3] Graduate student, Department of Civil Engineering, Konkuk University, Seoul, Korea
* Corresponding author; 1 Hwayang-dong, Gwangjin-gu, Seoul 143-701, Korea; parkys77@konkuk.ac.kr; Tel) +82-2-454-5882
[4] Assistant professor, Department of Civil Engineering, Konkuk University, Seoul, Korea
[5] Assistant professor, Department of Civil Engineering, Konkuk University, Seoul, Korea

(1993a, 1993b), Lotfi et al. (1994), Carol et al. (1997 and 2001), Hajjar et al. (1998), Soh et al. (1999), and Lei (2001) among others). Most of the models except for the early work of Katona (1983) that used Lagrange multiplier method adopted the fracture energy release concept to depict the localized deformation process on the basis of plastic flow theory with the Mohr-Coulomb failure criterion. However, even if the models are well established based on a robust continuum theory of plasticity, the values of parameters defining the constitutive equation have to be properly determined from the experimental results for a practical purpose. The parameters are bond strength, unbounded and bonded friction angles, residual level of friction angle, mode I fracture energy, mode II bonded fracture energy and unbonded slip-friction energy under different level of normal stress, and shape parameters defining geometrical shape of failure envelope. Little effort has been expended to extract the fundamental properties from post-peak measurements as only limited number of literature is available currently (Rabbat et al. (1985), Chajes et al. (1996), and Chiew et al. (1999)). Consequently, the lack of quantitative definition of parameters has hampered the numerical implementation to predict the behavior of steel-concrete composite structure and the further development of constitutive formulation of steel-concrete interface. This paper is concentrated on defining mechanical properties of constitutive parameters in steel-concrete interface.

Steel-concrete interface behavior is defined in the normal and tangential directions to the interface plane. Once reaching their critical states, tensile and shear behaviors in the normal and tangential directions, respectively, follow mode I type of debonding and mode II type of slip mechanisms of failure with the corresponding fracture energies dissipated. The slip on the interface strongly depends not only on the magnitude of the normal stress to the interface but also on the bonding condition of interface, bonded and unbounded, as Rabbat and Russell (1985) and Chiew et al. (1999) observed in their experiments performed on sandwich-typed steel-concrete interface specimen tests.

To identify constitutive parameters, a comprehensive constitutive model that accounts for the strong dependency of interface slip behavior on the bonding condition of interface is presented by modifying the hyperbolic Mohr-coulomb failure criterion of Lotfi et al. (1994) and Carol et al. (2001). The modification is obtained by expressing the bonded friction angle in terms of the unbonded friction angle and friction adjusting parameter. Values of parameters defining the model are determined through existing experimental results, geometry of failure envelope and sensitivity analyses. Only a few experimental results are available to evaluate mechanical properties of interface parameters because of highly pressure-sensitive nature of steel-concrete interface. Consequently, three existing experimental evidences of Rabbat and Russell (1985), Shakir-Khalil (1993 and 1994), and Chiew et al. (1999) are used to determine the values of parameters defining the model. Maximum value of unbonded friction parameter, residual level

of friction parameter and unbonded slip-friction energy are calculated from the unbonded tests of Rabbat and Russell (1985). Bond strength and mode I fracture energy are determined by geometrical relationships between parameters. Mode II bonded fracture energy and shape parameters of failure envelope are determined through sensitivity analyses performed based on experiments of Shakir-Khalil (1993) and Chiew et al. (1999). As a result, those values are applied to push-out tests of concrete-infilled rectangular steel columns with three different cases of interface lengths of Shakir-Khalil (1993 and 1994). Failure process of concrete-infilled rectangular steel column is discussed through the comparison of experimental measurements with numerical predictions.

2. Failure Criterion of Steel-Concrete Interface

Interface behavior between steel and concrete can be decomposed of mode I type of debonding and mode II type of slip. Based on test results of Rabbat and Russell (1985) and Chiew et al. (1999), the slip behavior is categorized into bonded and unbonded slips depending on the bonding condition of the interface. Numerous failure criteria to define the failure state of the interface have been presented based on the Mohr-Coulomb criterion including a linear representation of Plesha (1987), a parabolic representation of Stankowski et al. (1993), and a hyperbolic representation of Lotfi et al. (1994) and Carol et al. (1997). To incorporate the interface behavior of unbonded as well as bonded, the hyperbolic representation of failure envelope of Lotfi et al. (1994) and Carol et al. (1997) is modified as

$$F(\sigma_N,\ \sigma_T,\ \phi_b,\ b,\ k) = \sigma_T^2 - \phi_b^2 \left\{(\sigma_N - b)^2 - 2k(\sigma_N - b)\right\} \tag{1}$$

where σ_N is the normal stress, $\sigma_T = \sqrt{\sigma_L^2 + \sigma_M^2}$ is the tangential stress, b is the bond parameter, k is the curvature parameter that defines the curvature of the hyperbola. In Eq. (1), the bonded friction parameter ϕ_b that defines the friction angle of bonded interface is expressed as

$$\phi_b = \phi_u + \eta b \tag{2}$$

where ϕ_u is the friction parameter that defines the friction angle for the unbonded interface, and η is the friction angle adjusting parameter that adjusts the friction angle from unbonded to bonded. Geometry of the bond, curvature and friction parameters are shown in Fig. 1. Value of friction parameter in Eq. (2) is defined by Coulomb's friction rule and smaller than 1.0 for unbonded while greater than 1.0 for bonded according to the test results of Rabbat and Russell (1985) and Chiew et al. (1999). Thereby, the friction angle adjusting parameter η in Eq. (2) depicts the difference in frictional resistance between bonded and unbonded.

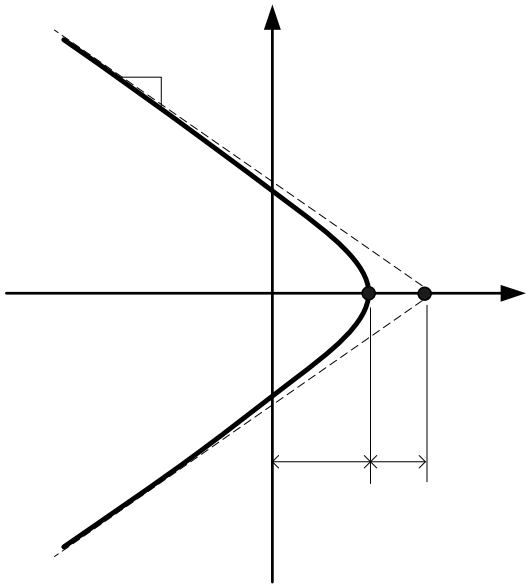

Fig. 1 Three-parameter failure envelope
of steel-concrete interface

Gradual contraction of failure envelope to simulate the progressive failure of interface is controlled by decreasing the values of three parameters ϕ, b, and k from the maximum values of $\phi^{\max}$, $b^{\max}$, and $k^{\max}$ to the residual values of ϕ^{res}, b^{res}, and k^{res}, respectively. The missing link between the maxima and residues of ϕ, b, and k is resolved by introducing mode I fracture energy G_f^I, mode II bonded fracture energy G_{fb}^{II} and unbonded slip-friction energy G_{fu}^{II}, and related plastic works of W_{PN} and W_{PT} in nomal and tangential

directions, respectively. To account for the effect of shear slip on debonding, the bond parameter b is approximated by independent energy fractions of plastic works to fracture energies of mode I and II similarly to Lotfi et al. (1994). However, friction and curvature parameters are approximated by an energy fraction related to mode II mechanism to account for the geometrical meaning of the two parameters on the failure surface.

$$
\begin{aligned}
b &= b^{res} + \left(b^{\max} - b^{res}\right)\left(1 - \beta_N \frac{W_{PN}}{G_f^I} - \beta_T \frac{W_{PT}}{G_f^{II}}\right) \\
\phi_b &= \phi^{res} + \left(\phi_b^{\max} - \phi^{res}\right)\left(1 - \alpha \frac{W_{PT}}{G_{fb}^{II}}\right) + \eta b \\
k &= k^{res} + \left(k^{\max} - k^{res}\right)\left(1 - \gamma \frac{W_{PT}}{G_{fb}^{II}}\right)
\end{aligned}
\tag{3}
$$

where β_N and β_T are the softening shape parameters of mode I and mode II, respectively, and α and γ are the shape parameters of friction and curvature, respectively. In case of debonding or unbonded slip behavior as shown in Fig. 2, the three parameters of Eq. (3) are modified as; 1) Debonding behavior: the bond parameter b governs the interface fracture process while the friction and curvature parameters of ϕ and k remain their maxima.

$$
\begin{aligned}
b &= b^{res} + \left(b^{\max} - b^{res}\right)\left(1 - \beta_N \frac{W_{PN}}{G_f^I} - \beta_T \frac{W_{PT}}{G_{fb}^{II}}\right) \\
\phi_b &= \phi_u^{\max} + \eta b, \qquad k = k^{\max}
\end{aligned}
\tag{4}
$$

2) Unbonded slip behavior: the friction and curvature parameters of ϕ and k diminish from the maxima to the residues while the bond parameter b remains its residual.

$$
\begin{aligned}
b &= b^{res}, \qquad \phi_u = \phi^{res} + \left(\phi_u^{\max} - \phi^{res}\right)\left(1 - \alpha \frac{W_{PT}}{G_{fu}^{II}}\right) \\
k &= k^{res} + \left(k^{\max} - k^{res}\right)\left(1 - \gamma \frac{W_{PT}}{G_{fu}^{II}}\right)
\end{aligned}
\tag{5}
$$

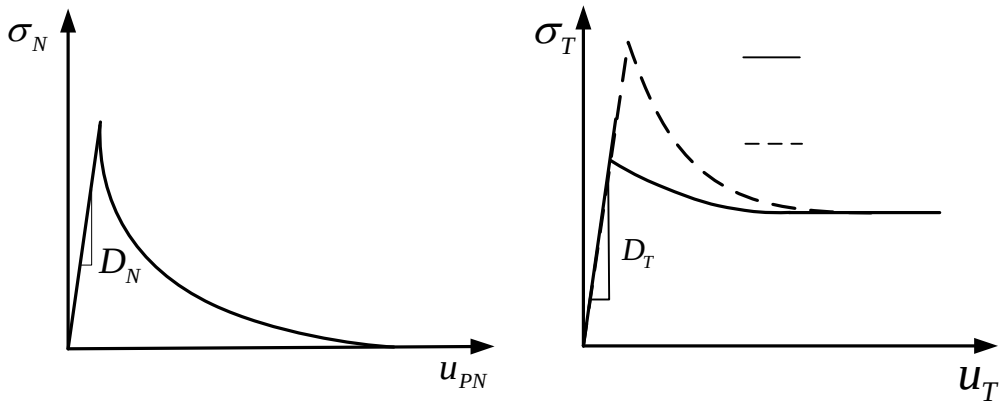

(a) (b)

Fig. 2 Stress-relative displacement relationships; (a) normal direction (b) tangential direction

Plastic works W_{PN} and W_{PT} in Eq. (3) that drive the interface failure process are defined in incremental sense as

$$dW_{PN} = \begin{cases} \sigma_N \cdot du_{PN} & \sigma_N \geq 0 \\ 0 & \sigma_N < 0 \end{cases} \qquad (6)$$
$$dW_{PN} = \left(\sigma_T - \sigma_T^{res}\right) \cdot du_{PT}$$

where the incremental plastic displacement in the current state $du_{PT} = \sqrt{du_{PL}^2 + du_{PM}^2}$ and the residual shear stress $\sigma_T^{res} = \pm\ \phi^{res}\sqrt{(\sigma_N - b^{res})^2 - 2k^{res}(\sigma_N - b^{res})}$.

3. Elasto-Plastic Interface Formulation

In the case of infinitesimal deformation, the total displacement rate vector $\dot{\mathbf{u}}$ may be decomposed into independent elastic and plastic components of $\dot{\mathbf{u}}_e$ and $\dot{\mathbf{u}}_p$, respectively, as $\dot{\mathbf{u}} = \dot{\mathbf{u}}_e + \dot{\mathbf{u}}_p$. Adopting a zero-thickness finite interface element in Fig. 3, stress-relative displacement in local coordinate is expressed as

$$\dot{\boldsymbol{\sigma}} = \mathbf{D}_{\mathrm{e}} : (\dot{\mathbf{u}} - \dot{\mathbf{u}}_{\mathrm{p}}) \tag{7}$$

where $\boldsymbol{\sigma} = \{\sigma_L \;\; \sigma_M \;\; \sigma_N\}^T$ and $\mathbf{u}_{\mathrm{e}} = \{u_L \;\; u_M \;\; u_N\}^T$, and subscripts L, M, and N denote the orthogonal directions of local coordinate. Elastic tangent operator $\mathbf{D}_{\mathrm{e}}$ in Eq. (6) is defined along each orthogonal direction as

$$\mathbf{D}_{\mathrm{e}} = \begin{bmatrix} D_L & 0 & 0 \\ 0 & D_M & 0 \\ 0 & 0 & D_N \end{bmatrix} \tag{8}$$

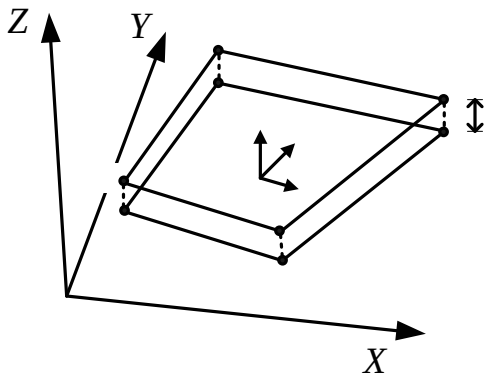

Fig. 3 Description of 8-node zero-thickness interface element

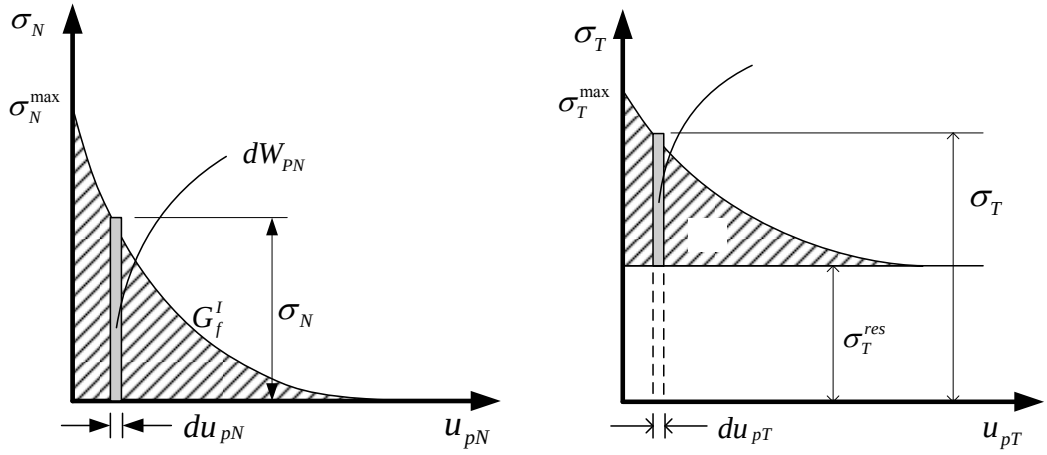

(a) (b)

Fig. 4 Incremental plastic work; (a) Mode I type (b) Mode II type

Adopting a nonassociated flow rule, the plastic displacement vector $\dot{\mathbf{u}}_p$ is defined in terms of

$$\dot{\mathbf{u}}_p = \dot{\lambda}\mathbf{m} \tag{9}$$

where $\dot{\lambda}$ and $\mathbf{m}$ are the plastic multiplier and the plastic flow vector, respectively. When the current stress with elastic increments of Eq. (7) violates the current state of failure criterion of Eq. (1), i.e. $F > 0$, the plastic flow occurs. Truncated Taylor series expansion of Eq. (1) leads to the linearized format of consistency to calculate the plastic multiplier $\dot{\lambda}$ where the failure function of Eq. (1) is expressed in an implicit rate form of $\dot{F}(\sigma_N,\ \sigma_T,\ \phi_b,\ b,\ k) = 0$

$$\dot{F} = \frac{\partial F}{\partial \boldsymbol{\sigma}} : \dot{\boldsymbol{\sigma}} + \frac{\partial F}{\partial u_p}\dot{u}_p = 0 \tag{10}$$

where equivalent plastic displacement $\dot{u}_p$ is obtained by Euclidean norm of $\dot{u}_p = \dot{\lambda}\|\mathbf{m}\|$. The plastic multiplier $\dot{\lambda}$, is obtained by substituting Eqs. (7) and (8) into (9) as

$$\dot{\lambda} = \frac{\mathbf{n} : \mathbf{D}_e : \dot{\mathbf{u}}}{-H\|\mathbf{m}\| + \mathbf{n} : \mathbf{D}_e : \mathbf{m}} \tag{11}$$

where the gradient $\mathbf{n} = \partial F / \partial \boldsymbol{\sigma}$, $\mathbf{m} = \partial Q / \partial \boldsymbol{\sigma}$ and Q is plastic potential. The hardening parameter H in Eq. (10) is calculated by the chain rule of differentiation as

$$H = \frac{\partial F}{\partial \phi_b}\frac{\partial \phi_b}{\partial \phi_u}\frac{\partial \phi_u}{\partial W_{PT}}\frac{\partial W_{PT}}{\partial u_{PT}} + \left(\frac{\partial F}{\partial \phi_b}\frac{\partial \phi_b}{\partial b} + \frac{\partial F}{\partial b}\right)\left(\frac{\partial b}{\partial W_{PN}}\frac{\partial W_{PN}}{\partial u_{PN}} + \frac{\partial b}{\partial W_{PT}}\frac{\partial W_{PT}}{\partial u_{PT}}\right) + \frac{\partial F}{\partial k}\frac{\partial k}{\partial W_{PT}}\frac{\partial W_{PT}}{\partial u_{PT}} \tag{12}$$

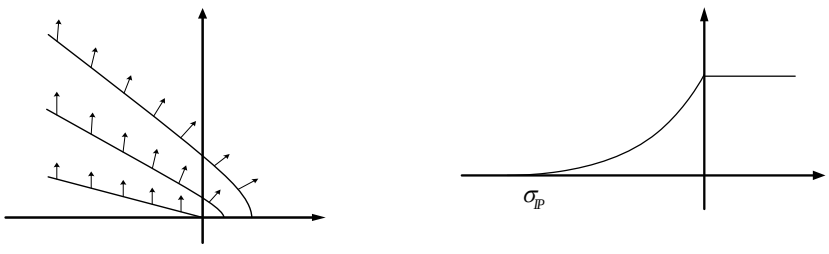

(a) (b)

Fig. 5 Nonassociated plastic flow; (a) Direction of plastic flow on failure surface

(b) Nonassociativity intensity factor f_I

When shear slip proceeds on interface, dilatancy of interface decreases due to abrasion of the residue and confining pressure acting on the interface along normal direction. Nonassociated plastic flow rule is adopted to control the excessive dilatancy that is commonly encountered in a computational plasticity (see Fig. 5(a)). In this paper, direction of non-associated plastic flow vector $\mathbf{m}$ is determined through the way of adjusting associated plastic flow vector $\mathbf{n}$ as the case of conventional plasticity of Lee and Willam (1995). Along the line of concept, nonassociativity intensity factor f_I is introduced as a function of nonassociativity inflection parameter I_P which designates normal stress value of not having the flow component along normal stress direction on the failure surface as shown in Fig. 5(b).

$$\begin{aligned} &\frac{\partial Q}{\partial \sigma_L} = \frac{\partial F}{\partial \sigma_L}, \quad \frac{\partial Q}{\partial \sigma_M} = \frac{\partial F}{\partial \sigma_M} \\ &\frac{\partial Q}{\partial \sigma_N} = \left(\frac{\partial F}{\partial \sigma_N} \right) f_I \left(\frac{\phi - \phi^{res}}{\phi^{\max} - \phi^{res}} \right) \end{aligned} \tag{13}$$

where nonassociativity intensity factor f_I is defined as $f_I = \left\{ (\sigma_N - \sigma_{IP}) / \sigma_{IP} \right\}^2$.

The elastoplastic tangent operator, $\mathbf{D}_{\text{ep}}$, to link stresses and relative displacements is obtained by substituting the plastic multiplier of Eq. (11) into (7) as

$$\mathbf{D}_{\text{ep}} = \mathbf{D}_{\text{e}} - \frac{\mathbf{D}_{\text{e}} : \mathbf{m} \otimes \mathbf{n} : \mathbf{D}_{\text{e}}}{-H \left\| \mathbf{m} \right\| + \mathbf{n} : \mathbf{D}_{\text{e}} : \mathbf{m}} \tag{14}$$

4. Parameter Values of Steel-Concrete Interface

Values of parameters defining the presented model were determined through existing experimental results, geometry of failure envelope and sensitivity analyses. Due to limited number of experimental works, three existing experimental results of Rabbat and Russell (1985), Shakir-Khalil (1993), and Chiew et al. (1999) were adopted to determine the values of parameters defining the presented model.

4.1 Experiments of Rabbat et al. (1985), Chiew et al. (1999), Shakir-Khalil (1993)

Figure 6(a) shows a test specimen for steel-concrete interface tested by Rabbat et al. (1985). In their experiments, concrete block with 150mm thickness, 340mm width and 610mm length was cast and cured on steel plate with 25mm thickness, 360mm width and 710mm length of Grade 70 according to A516 of ASTM. Surface of the plate was treated according to SSPC-SP2-63 of Steel Structures Council Specifications. After 7 days of curing, concrete formwork placed on the plate was removed and concrete was cured in the laboratory with $23^{\circ}C$ temperature and 50% humidity. At 28 days of age when nominal strength of concrete reached 30MPa, bonded slip test with constant confining pressure of $\sigma_N = 0.056$ MPa was performed by applying slip force until the interface was completely failed. Then, unbonded slip test was performed for the tested specimen in a same manner but confining pressure of $\sigma_N = 0.41$MPa.

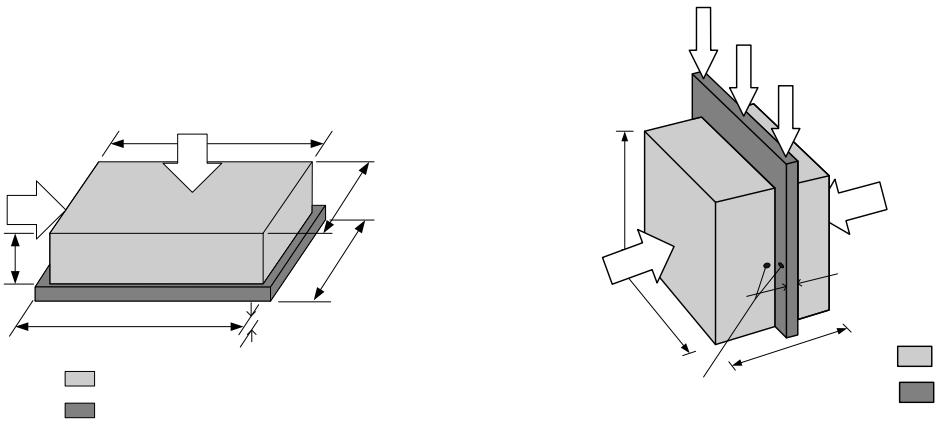

Fig. 6 Descriptions of test specimens of; (a) Rabbat et al. (1985) and (b) Chiew et al. (1999).

Figure 6(b) shows a test specimen of Chiew et al. (1999) where 20mm thick steel plate was placed between two concrete blocks with 150mm width, 150mm height and 65mm thickness. To investigate the effect of confining pressure on interface behavior, three different levels of confining pressure including $\sigma_N = 0.5$MPa , 1.0MPa and 1.5MPa were applied to specimens. In case of $\sigma_N = 1.5$MPa , unbonded slip test with $\sigma_N = 1.5$MPa was performed for the same specimen that was already tested for bonded slip to observe the difference between bonded ad unbounded.

Shakir-Khalil (1993) performed 40 tests of concrete-infilled rectangular steel column to determine the failure strength of a steel-concrete interface. To investigate the effect of the number of shear studs on the failure strength, specimens with 2, 4, and 6 shear studs were tested as well as those with no

shear stud. All the specimens had 150×150 mm cross section and 5mm thick steel plate. Three different interface lengths of 200mm, 400mm and 600mm were considered to investigate the effect of the interface area on the failure strength.

Constitutive parameters of steel-concrete interface including six of mechanical properties and three of shape parameters of failure envelope were evaluated based on the three test results and sensitivity analysis. Mechanical properties of the maximum value of friction parameter $\phi_u^{\max}$, the residual value of friction parameter ϕ^{res}, and unbonded slip-friction energy G_{fu}^{II} were determined from the test results of Rabbat et al. (1985). Friction angle adjusting parameter η and mode II bonded fracture energy G_{fb}^{II} were determined through sensitivity analyses performed based on the test results of Chiew et al. (1999). Bond strength $b^{\max}$ was calculated by geometrical relations of three parameters defining a failure envelope function. Finally, nonassociativity inflection parameter I_p was determined through sensitivity analyses for the test results of Shakir-Khalil (1993).

4.2 Determination of Interface Parameter Values

- Maximum value of unbounded friction parameter $\phi_u^{\max}$, residual friction parameter ϕ^{res}, unbonded slip-friction energy G_{fu}^{II}

Rabbat and Russell (1985) obtained the maximum values of average shear stresses of $\sigma_{Tb}^{\max}=0.41$ MPa and $\sigma_{Tu}^{\max}=0.28$ MPa from bonded and unbonded tests, respectively, and residual and maximum values of friction parameter of $\phi^{res}=0.57$ and $\phi_u^{\max}=0.7$, respectively. Table 1 summarizes the test results of Rabbat and Russell where the residual stress denotes the stress to which the level of average shear stress converges as the slip increases far enough, as shown in Fig. 7. Unbonded slip-friction energy G_{fu}^{II} was obtained to be $0.21\sigma_N$ N$\cdot$mm/mm^2 by measuring the area of Test-3 curve in Fig. 7.

Table 1 : Experimental results of Rabbat et. al. (1985)

No.	Comp. strength (MPa)	Averaging shear stress (MPa)				Friction coefficient			
		Bonded case		Unbonded case					
		Max.	Ave.	Max.	Res.	Max.	Ave.	Min.	Ave.
1	25.0	0.46	0.41	0.28	0.23	0.68	0.69	0.56	0.57
2	25.6	0.37		0.32	0.24	0.77		0.58	
3	25.6	0.4		0.25	0.23	0.62		0.57	

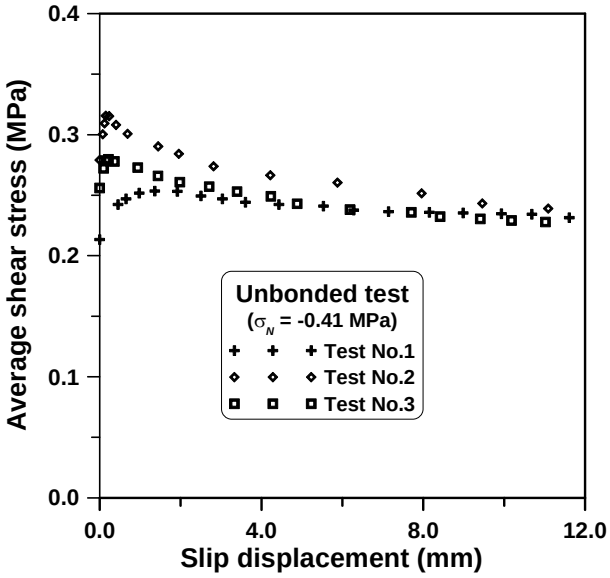

Fig. 7 Unbonded slip test results of Rabbat et. al. (1985)

- Curvature parameter $k^{\max}$ and bond strength $b^{\max}$

A linear equation of $\phi_b^{\max}(|\sigma_N| + b^{\max} + k^{\max}) = \sigma_{Tb}^{\max}$ to define bond strength $b^{\max}$ was obtained in terms of σ_N, $\phi_b^{\max}$, $k^{\max}$, and $\sigma_{Tb}^{\max}$ from the geometry of the maximum failure envelope shown in Fig. 8. Substituting $\phi_b^{\max} = \phi_u^{\max} + \eta\, b^{\max}$ of Eq. (2) and $b^{\max} = 2\, k^{\max}$ obtained from the sensitivity analysis into the equation, a second order polynomial equation to calculate $b^{\max}$ is obtained as $\eta(b^{\max})^2 + [\phi_u^{\max} + \eta(|\sigma_N| + k^{\max})]\, b^{\max} + \phi_u^{\max}(|\sigma_N| + k^{\max}) - \sigma_{Tb}^{\max} = 0$ where $\eta = 6.5$ was obtained from sensitivity analysis. Bond strength $b^{\max}$ can be readily calculated when the value of σ_N is specified which is the normal stress corresponding to average shear stress $\sigma_{Tb}^{\max}$.

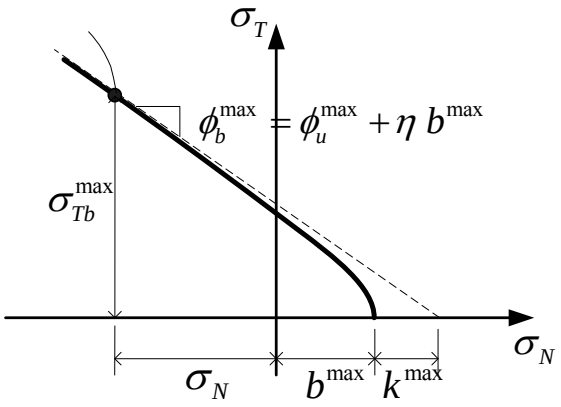

Fig. 8 Geometrical description of interface parameters

- Mode I fracture energy G_f^I, mode II fracture energy G_{fb}^{II}, friction angle adjusting parameter η, and nonassociativity inflection parameter I_p

Values of mode I fracture energy G_f^I, mode II bonded fracture energy G_{fb}^{II}, friction angle adjusting parameter η, and nonassociativity inflection parameter I_p were determined through the sensitivity analyses performed based on the test results of Chiew et al. (1999). Three levels of confining pressure were considered including $\sigma_N = 0.5$, 1.0, and 1.5 MPa as the case of tests. The parameter values of $\phi_u^{\max} = 0.7$, $\phi^{res} = 0.57$, and $G_{fu}^{II} = 0.21\sigma_N$ N·mm/mm^2 were used in the analysis which were obtained based on the test results of Rabbat and Russell (1985). Through the sensitivity analyses, the maximum values of shear stress $\sigma_{Tb}^{\max}$ corresponding to each confining pressure were 0.79, 1.51, and 2.25 MPa, respectively, and bond strengths $b^{\max}$ were obtained to be 0.086, 0.096, and 0.108 MPa, respectively. Based on the values, the values of G_{fb}^{II}, G_f^I, η, and I_p were obtained to be $(6.5\sigma_N + 0.12)$ N·mm/mm^2, 0.2 N·mm/mm^2, 6.5, and –0.25 MPa, respectively. Figs. 8-16 show sensitivity analysis results and compare those with experimental results corresponding to each interface parameter.

4.3 Prediction of the Test Results of Shakir-Khalil (1993)

The determined parameter values were used to predict the interface behavior of concrete-infilled rectangular steel column tests of Shakir-Khalil (1993). Figure 17 shows the undeformed and deformed shapes of the quarter model of the specimens with three different interface lengths of 200, 400, and 600mm, i.e. in the ratio of 1:2:3. Three dimensional 8-node brick element, 4-node Mindlin-type shell element and 8-node zero-thickness element were used for finite element modeling of concrete, steel plate and interface, respectively. A conventional three dimensional elasto-plastic constitutive model based on four-parameter failure criterion and von Mises failure criterion were used to depict material nonlinearities of infilled-concrete and steel plate, respectively. Material properties and interface parameters used in the analysis are summarized in Table 2.

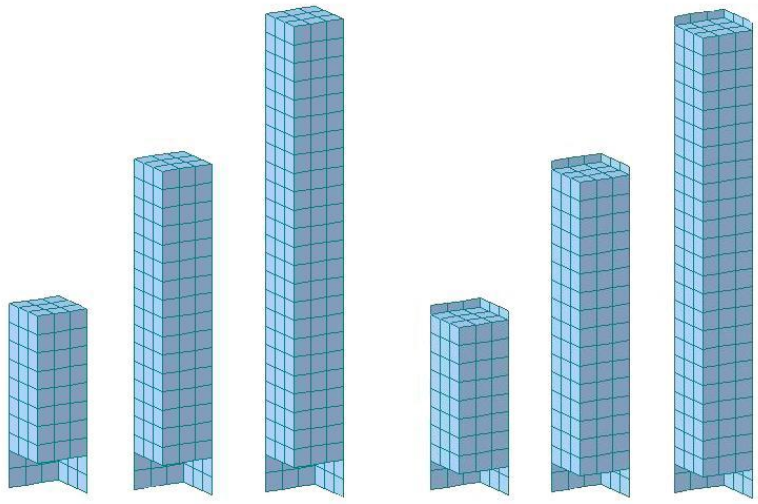

(a) (b)

Fig. 17 Deformed and undeformed geometries of Shakir-Khalil's test specimens with 200, 400 and 600mm interface lengths ; (a) undeformed geometry (b) deformed geometry

Table 2 Parameter values for concrete-infilled steel column

Properties		values	Properties		values
Conc.	E_c (MPa)	27,900	Steel	E_s	196,000
	ν_c	0.18		ν_s	0.3
	f_{ck}	41		f_y	295
	f_t	4.1			
D_T ($\mathrm{N/mm^3}$)		30	η		6.5
D_N ($\mathrm{N/mm^3}$)		10000	α		1.0
$\phi_u^{\max}$		0.7	β_I		50.0
ϕ^{res}		0.57	β_{II}		1.0
$b_{\max}$		0.062	γ		1.0
b^{res}		0	I_p		-0.25
$k^{\max}$		0.031	G_f^I ($\mathrm{N\cdot mm/mm^2}$)		$0.21\sigma_N$
k^{res}		0	G_{fb}^{II} ($\mathrm{N\cdot mm/mm^2}$)		$(6.5\sigma_N + 0.12)$

Figure 18 compares the measured and predicted results of the applied load vs. slip displacement relationship for the three different interface length cases. The predicted results preserve agreement with the measured results except for the shortest interface length case of 200mm where the measured peak load is much higher than the predicted one. It is shown in the predicted results that peak loads corresponding to each interface length case are approximately in the ratio of 1:2:3 which are similar ratio to interface lengths of 200, 400, 600mm. However, the ratio is not preserved for the measured results where the peak load of 200mm gets close to that of 400mm. In addition, post-peak behaviors for each interface length case of the predicted results are similar to one another and residual levels are in the ratio of 1:2:3. Based on the observations obtained from the predicted results, it is revealed that the interface resistance of concrete-infilled rectangular hollow section to a pushout force is proportional to interface area, which means that slip energy release rate in interface is constant regardless to interface area in

this particular case. However, it may be controversial because the measured results show that changing the interface length does not seem to have a direct and proportional effect on the load-carrying capacity of the specimens. Shakir-Khalil (1993) mentioned that the reason of not existing direct relation between the interface resistance and area could be interface condition, local imperfections and shrinkage of infilled concrete. Considering interface conditions is beyond the scope of current paper and additional test results are required in other to establish the relationship between the interface resistance and surface conditions. Restricting the scope of interests into the performance of current constitutive model and parameters, nevertheless, it is worth while to discuss a constant value of slip energy release rate, which could be acceptable in a mechanical sense, within the limitation of the interface behavior having uniform mechanical condition of interface.

Figure 20 compares the longitudinal strain values measured at the four locations of the 600 mm interface length specimen with the predicted strain values. Locations of strain gages attached on the specimen are shown in Fig. 19. Both of the measured and predicted results show the gradual strain increase in the steel wall from the top of specimen to the base. This is due to the load transfer from the core concrete to the steel hollow section through the slip resistance acting along the interface. Slopes of load vs. strain curves of gages 1 and 2 gradually increase upward while those of gages 3 and 4 gradually decrease downward as the applied load level approaches its peak. These slope changes indicate that the interface slip in gages 1 and 2 occurred far before reaching peak, the interface slip in gage 3 occurred in the vicinity of peak, and the interface slip in gage 4 led to the sudden global failure, which results in strain recovery in steel. The measured and predicted results show good agreements in depicting the failure process as well as in comparing absolute values.

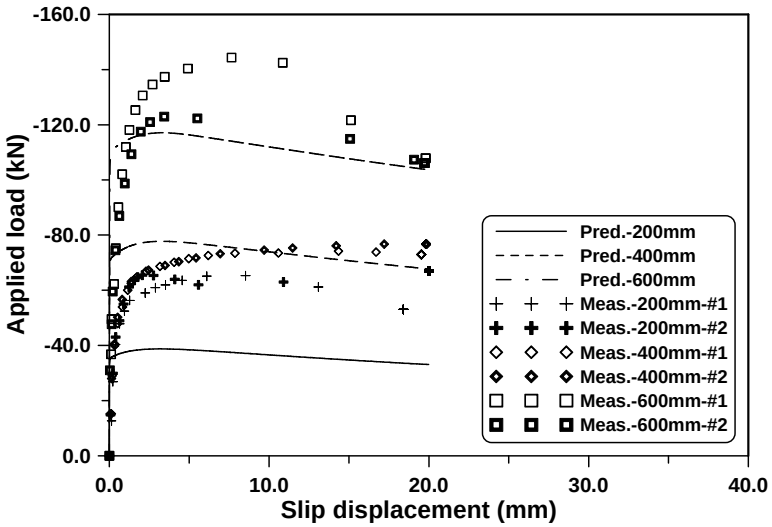

Fig. 18 Measured and predicted slip displacements of Sharkr-Khalil's experiments

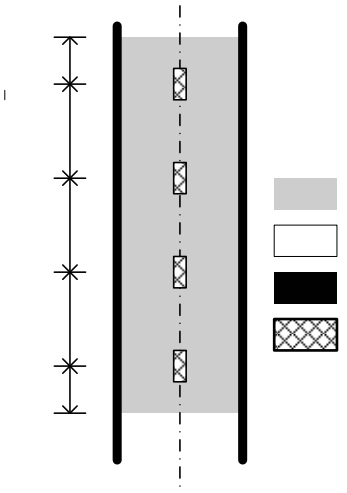

Fig. 19 Locations of strain gages attached on steel plate.

5. Conclusion

A way to evaluate the parameter values of steel-concrete interface model were illustrated when the constitutive formulation is based on the Mohr-Coulomb type failure criterion combined with the fracture energy concept to depict progressive interface failure. For this purpose, a comprehensive constitutive model to describe bond and slip failures of the interface was presented which has capability of depicting the dependency of interface behavior on bonding condition of bonded or unbonded. As the result, values of nine interface parameters were determined based on three experimental results, geometry of failure criterion and sensitivity analyses. Values of the three parameters of the maximum value of unbounded friction parameter $\phi_u^{\max}$, residual friction parameter ϕ^{res}, and unbonded slip-friction energy G_{fu}^{II} were determined based on the experimental results of Rabbat and Russel (1985). Values of the two parameters of curvature parameter $k^{\max}$ and bond strength $b^{\max}$ were determined based on the geometrical relationship of failure criterion. Values of the four interface parameters of mode I fracture energy G_f^I, mode II fracture energy G_{fb}^{II}, friction angle adjusting parameter η, and nonassociativity inflection parameter I_p were calculated by sensitivity analysis performed based on Chiew et al. (1999). The parameter values were applied to predict the slip resistance of concrete-infilled rectangular steel column under pushout force. It was observed through the numerical failure prediction that the interface resistance of concrete-infilled rectangular hollow section to a pushout force was proportional to interface area leading to constant slip energy release rate

regardless of interface area for the particular case. In addition, it was assured that an enough load transfer occurs between steel and concrete until reaching global failure and upon reaching peak load level, the failure is sudden and results in strain recovery in steel part that means energy release strained in steel as well as in infilled-concrete.

Acknowledgement

This search was supported by a grant from Construction Technology Innovation Program funded by Ministry of Construction & Transportation of Korean government.

References

1. Carol, I., Lopez, C.M. and Roa, O. (2001) Micromechanical Analysis of Quasi-Brittle Materials Using Fracture-based Interface Elements. Int. J. for Num. Meth. in Engrg., Vol. 52, pp. 193-215.

2. Carol, I., Prat, P. C. and Lopez, C.M. (1997) Normal/Shear Cracking Model : Application to Discrete Crack Analysis. J. of Engrg. Mech., ASCE, Vol. 123, No. 8, pp. 765-773.

3. Chajes, M.J., Finch, W.W.Jr., Januszka, T.F., and Thomson, T.A.Jr. (1996) Bond and force transfer of Composite Material Plates Bonded to Concrete. ACI Struct. J., Vol.93, No.2, pp.208-217.

4. Chiew, S.P., Dong, Y.X. and Sho, C.K. (1999) Concrete-Steel Plate Interface Characteristics for Composite Construction. Proc., 7th Int. Conf. on Computing Developments in Civ. and Struc. Engrg. (CIVIL-COMP99), B. Kumar and B.H.V. Topping, eds., Civil-Comp, Edinburgh, pp. 35-40.

5. Hajjar, J.F., Schiller, P.H., and Molodan, A. (1998) A Distributed Plasticity Model for Concrete-filled Steel Tube Beam-Coulmns with Interlayer Slip, Engineering Structures, Vol. 20, No. 8, pp.663-676.

6. Katona, M.G. (1983) A Simple Contact-Friction Interface Element with Applications to Buried Culverts. Int. J. for Num. and Anal. Meth. in Geomech., Vol. 7, pp. 371-384.

7. Lee, Y.-H., and Willam, K. (1995), Anisotropic Vertex Plasticity Formulation of Concrete In-plane Stress." J. of Engrg. Mech., ASCE, 123(7), pp.714-726.

8. Lei, X.Y. (2001) Contact Friction Analysis with a Simple Interface Element. Computer Methods in Appl. Mech. and Engrg., Vol.190, pp.1955-1965.

9. Lotfi, H.R. and Shing, P.B. (1994), Interface Model Applied to Fracture of Masonry Structures, J. of Struc. Engrg., ASCE, Vol. 120, No. 1, pp. 63-79.

10. Plesha M.E. (1987) Constitutive Models for Rock Discontinuities with Dilatancy and Surface Degradation. Int. J. for Num. and Anal. Meth. in Geomech., Vol. 11, pp. 345-362.

11. Rabbat, B.G. and Russell, H.G. (1985), Friction Coeffcient of Steel on Concrete or Grout, Journal of Struc. Engrg., ASCE, Vol. 111, No. 3, March, pp. 505-515

12. Shakir-Khalil, H. (1993) Pushout Strength of Concrete-filled Steel Hollow Sections, The Structural Engineer, Vol. 71, No. 13, pp. 230-233.

13. Shakir-Khalil, H. (1993) Resistance of Concrete-filled Steel Tubes to Pushout Forces, The Structural Engineer, Vol. 71, No. 13, pp. 234-243.

14. Shakir-Khalil, H. , and Hassan, N.K.A. (1994) Push-out Resistance of Concrete-filled Tubes. Tubular Structures VI, Grundy, P., Holgate, A., and Wong. W. (eds), Melbourne, Australia, A. A. Balkema, Rotterdam, The Netherlands, pp.285-291.

15. Soh, C.K., Chiew, S.P., and Dong, Y.X. (1999) Damage Model for Concrete-Steel Interface. J. of Engrg. Mech., ASCE, Vol.125, No. 8, pp.979-983

16. Stankowski, T., Runesson, K., and Sture, S. (1993) Fracture and Slip of Interfaces in Cementitious Composites. I: Characteristics. Journal of Engrg. Mech., ASCE, Vol. 119, No. 2, pp. 315-327.

17. Stankowski, T., Runesson, K., and Sture, S. (1993) Fracture and Slip of Interfaces in Cementitious Composites. II : Implementation. Journal of Engirg. Mech., ASCE, Vol. 119, No. 2, pp. 315-327.

18. Thomann, M., and Lebet, J.-P. (2008) A Mechanical Model for Connections by Adherence for Steel-Concrete Composite Beams. Engineering Structures, Vol.30, pp.163-173.

19. Zhu, X.Q., and Law, S.S. (2007) A Concrete-Steel Interface Element for Damage Detection of Reinforced Concrete Structures. Engineering Structures, Vol.29, pp.3515-3524.